Photoemission from activated gallium arsenide. I. Very-high-resolution energy distribution curves

H.-J. Drouhin, C. Hermann, and G. Lampel
Laboratoire de Physique de la Matière Condensée, Ecole Polytechnique, 91128 Palaiseau, France
(Received 17 July 1984)

The energy distribution curves (EDC's) of the photoelectrons emitted from the (100) face of a *p*-type doped ($\sim 10^{19}$ cm^{-3}) GaAs crystal, activated to negative electron affinity in ultrahigh-vacuum conditions, is investigated. The study is performed at 300 and 120 K under well-focused Kr^+-laser excitation and with a very-high-energy resolution (20 meV). The analysis of the EDC's as a function of the photon energy, mainly at low temperature, is shown to provide a very direct picture of the GaAs band structure away from the Brillouin-zone center. The experimental results are well fitted by a spherical, nonparabolic $\vec{k}\cdot\vec{p}$ perturbation calculation of the coupled conduction and valence bands, for electron kinetic energies up to 1 eV in the central Γ valley. The essential role played by the subsidiary L and X minima in the energy relaxation and photoemission processes is evidenced. The main contribution to the total emitted current is due to electrons which were thermalized in the bulk Γ minimum and have lost an average energy $\simeq$130 meV in the band-bending region prior to emission into vacuum. The band-bending value is shown to be $\geq$0.5 eV. The yield and time evolution of GaAs photocathodes are discussed. This detailed study leads to a reexamination of the pioneer work of L. W. James and J. L. Moll [Phys. Rev. **183**, 740 (1969)] and to a good understanding of the photoemission properties of activated GaAs.

I. INTRODUCTION

Cesium and oxygen coadsorption on a gallium arsenide crystal has proved to produce very-high-efficiency photocathodes in the visible and near-infrared spectrum.[1] For more than a decade, negative-electron-affinity (NEA) photocathodes have been widely used in photomultiplier tubes and the activation procedure, developed for industrial purpose, is well known.[2] For some years, NEA GaAs photocathodes under circularly polarized light excitation (i.e., optical pumping) have found important applications as polarized electron sources[3–8] in high-energy physics,[9–13] molecular and atomic physics,[14,15] and surface physics.[16] More recently,[17] we have shown that, under proper operating conditions, GaAs photocathodes provide intense and quasimonochromatic electron beams and in this way greatly improve the performance of available electron sources. Such sources are now used in collision physics experiments.[18]

Photoemission of NEA GaAs was carefully studied in the pioneer work of James and collaborators[19–21] who deduced some transport properties from the analysis of the energy distribution curves (EDC's), i.e., the emitted-photoelectron intensity versus electron kinetic energy for different photon energies. Hot-photoluminescence experiments on *p*-type GaAs at liquid-nitrogen temperature have evidenced the importance of nonthermalized electrons in the bulk crystal.[22] Although GaAs photocathodes are very commonly used as spin-polarized electron sources, little work on the physics of their photoemission has been published over the last ten years.

Using an optimized electron spectrometer, we have performed very-high-resolution energy analyses of the electrons emitted by an activated GaAs crystal.[23] Laser excitation allows one to obtain intense photoemission from a well-defined emitting area. Under optical-pumping conditions, we have also measured the spin polarization of the photoelectrons as a function of their kinetic energy. Preliminary results are reported in Refs. 17 and 24.

This paper (hereafter referred to as I) is devoted to the study of the EDC's as a function of the excitation energy mainly at a temperature close to that of liquid nitrogen. When a photon of energy $h\nu$ is absorbed, electrons are promoted from the valence bands into the conduction band at different initial kinetic energies. For $h\nu \leq 3$ eV, they are only excited in the central Γ valley of the conduction band. A very minute fraction of these electrons is emitted into the vacuum without any energy loss. These electrons appear in the EDC's as starting points of well-defined structures which may be tracked by varying $h\nu$. However, most of the photoexcited electrons suffer energy relaxation in the Γ minimum or, more probably—when energetically possible—in the L and X side valleys of the conduction band. During the energy relaxation, they always have a finite probability of escaping into the vacuum: This gives rise to plateaus in the EDC's on the low-energy side of the starting points. When sufficient energy has been lost, the electrons reach the different minima where they accumulate. A small fraction of the electrons relaxed in the side minima may escape into vacuum either directly, producing energy-independent starting points of specific structures in the EDC's or after energy relaxation in the band-bending region near the surface, giving rise to broad plateaus. Most of the photoexcited electrons reach the bottom of the conduction band in the bulk, i.e., the Γ minimum, where they thermalize at an effective temperature depending on the excitation conditions and on the lattice temperature. They diffuse then to the surface

through the band-bending region and suffer additional energy relaxation with a mean energy loss of about 130 meV before escaping into vacuum giving rise to the prominent "Γ peak" of the EDC's. When $h\nu$ is varied, the EDC's are continuously modified and the evolution of each structure permits its identification in relation with the band structure.[25]

After describing the experimental conditions of our measurements in Sec. II, we briefly recall the theoretical background on GaAs band structure and NEA photoemission in Sec. III. In Sec. IV we discuss in detail our high-resolution EDC's and present a reinterpretation of the data of James and collaborators.[19–21]

In the following paper[26] (hereafter referred to as II) we shall study polarization versus energy distribution curves (PEDC's). The PEDC's point out the drastic effect of spin relaxation as a function of kinetic energy and confirm the EDC structures. We shall then compare hot-luminescence polarization to photoemission data to achieve a more complete understanding of the spin- and energy-relaxation mechanisms during the escape process. In the last section of II the physics of monochromatic and polarized electron sources will be discussed using the concepts developed in I and II.

II. EXPERIMENT

A schematic sketch of the experimental setup is shown in Fig. 1. The crystal holder is mounted on a 50-mm translation stage. This permits either to prepare the sample away from the electron optics or to position it precisely for the experiment. The photocathode is then facing a 90° cylindrical deflector (the rotator) which allows light excitation normal to the crystal surface. After deceleration, the electrons are energy selected by another identical electrostatic deflector (the selector) the revolution axis of which is orthogonal to that of the rotator. In optical-pumping experiments, the spin-orientation axis of the photoelectrons is parallel to the direction of light excitation. In our geometry, it is thus perpendicular to the propagation direction of the electron beam after energy selection: This configuration is necessary for spin-polarization measurements using a Mott polarimeter.

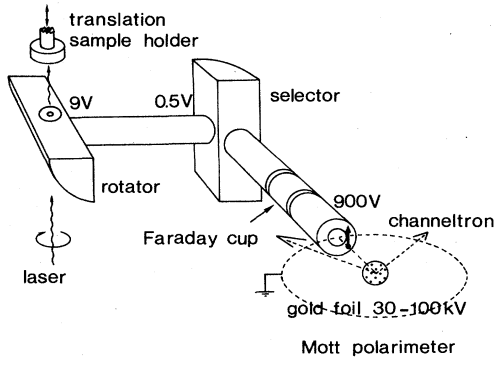

FIG. 1. Schematic diagram of the apparatus. The photocathode, mounted on a translation displacement, is illuminated normal to its surface. The emitted electrons are successively 90° deflected in the rotator, decelerated and energy analyzed in the selector. The indicated bias voltages correspond to a 20-meV resolution. The electrons can either be collected into the Faraday cup, which provides the EDC's, or reaccelerated to the Mott polarimeter, where their spin orientation is measured (see Sec. II of II). For a circularly polarized laser excitation, the electron spins are oriented along the heavy arrow.

A. Electron optics

1. Energy selector

The photoelectrons are energy selected by a 90° electrostatic cylindrical deflection selector (CDS)[27,28] of Marmet-Kerwin type.[29] The internal and external grid radii are, respectively, $R_I = 10$ mm and $R_E = 15$ mm. The slits, centered on the mean radius $R_0 = (R_E R_I)^{1/2}$, have a width $s = 0.5$ mm. The selector is used in the constant-energy mode, in which the cathode bias voltage is scanned. This mode leaves unchanged all electrode biasing potentials and leads to a more uniform transmission. We select electrons which would have zero kinetic energy in the zero electrostatic potential and, consequently, apply to the cathode, the voltage

$$V_{\text{cathode}}(E) = (E + \Phi - \Phi_{\text{selector}})/e \quad (1)$$

to select electrons of kinetic energy E out of the cathode and near the surface. In this formula, Φ (respectively, Φ_{selector}) is the cathode (respectively, selector) work function and $-e$ is the electron charge. For small entrance angles, a CDS has a triangular transmission function of full width at half maximum (FWHM) $\Delta E = E_0 s/R_0$, where E_0 is the electron kinetic energy at the selector. In our design $\Delta E \simeq 4.10^{-2} E_0$ and since we work at $E_0 = 0.5$ eV, $\Delta E \simeq 20$ meV. The resolution has been experimentally tested by an original method using the thermionic emission of a tungsten cathode.[23,30] To achieve such a performance, care has been taken for all limiting resolution factors. The electron beam is collimated to a 4° half-angle divergence before energy analysis and the stray magnetic fields are shielded to less than 1 μT. In order to reduce contact potential inhomogeneities, the whole low-energy electron optics is made of a gold-plated nonmagnetic alloy (AP4 Arcap). The fluctuations of all electrode biasing voltages are reduced to a very low level (~ 1 mV). Charged adsorbates are often a cause of troubles in very-low-energy electron optics: After installation, the whole setup had to be baked up to 350 °C for 1 week to become completely free of long-term drifts in operation. Moreover, a 12-W resistive heater located inside the ultra high-vacuum (UHV) chamber can bake the spectrometer up to 150 °C while the pressure remains in the low 10^{-10}-Torr range. Due to all these precautions the measurements are highly reproducible, as can be tested from the conservation of the correspondence between the electron energy and cathode voltage over very long periods (months), and the selector output current ranges between 10^{-2} and 10^{-3} of the total emitted current.

A very important problem is that of energy calibration: Although the CDS grid work function does not appreciably vary over long times it cannot be easily measured with accuracy. The best solution is to take advantage of

some EDC structures occurring at well-defined energies. We will see that a GaAs photocathode provides such accurate energy references (see Sec. IV A 1).

2. Electron rotator

The rotator permits the illumination of the photocathode normally to its surface through a 4-mm-diameter hole in the CDS external collector. The entrance slit is designed to be directly used as an anode. Because of the low rotator biasing voltages, the system must be used with a relatively low emitted current: In our experiments, we generally restrict it to $\sim 1\ \mu$A.

3. Additional electron optics

A three-cylinder retarding optics ensures proper imaging of the emitting point on the selector entrance slit. An eight-element accelerating optics transports the energy selected electrons towards the Mott polarimeter which is used to measure the electron spin polarization (see Sec. II of II). By suitably modifying the bias voltages of the latter transport optics, the beam may be collected on a specially designed electrode which acts as an efficient Faraday cup. To obtain the EDC's the current is measured with a picoammeter; the EDC derivatives are simply recorded by adding a small additional modulation (~ 15 mV peak to peak) to the photocathode bias voltage. The transmitted current is then detected with a lock-in amplifier. We operate at a modulation frequency ~ 750 Hz and are able to observe current variations of approximately 10^{-14} A.

4. Power supplies

A single power supply defines all electron optics biasing potentials by means of amplifiers: This minimizes line pickup. Furthermore, the energy resolution ΔE can be varied from 100 to 20 meV without uncontrolled modifications of the electron trajectories (which might lead to surface charge effects on some parts of the optics and, consequently, to long-term drifts).

B. Light excitation

Two distinct light sources are used: a 2.5-mW He-Ne laser at 1.96 eV and a krypton-ion laser with discrete lines in the visible and near-infrared regions. The He-Ne laser is also used as an alignment reference. Both are focused on the sample by a 300-mm focal lens and may be circularly polarized by a computer-controlled Babinet-Soleil compensator. Great care has been taken to produce a small and homogeneous spot (diameter ~ 0.5 mm), in particular, the Kr^+ laser is collimated by a small adjustable diaphragm. This provides a well-defined emitting area for the electron optics and prevents averaging over regions with different work functions. Neutral filters are used to maintain the total emitted current in the 1-μA range.

C. Samples

1. Sample holder

The sample holder consists of a thin tantalum disk, welded on a molybdenum ring, against which the GaAs crystal is clamped. It can be heated by radiation from a filament mounted behind the tantulum disk. A precise adjustment of the temperature is obtained by additional electron bombardment. The total power needed is about 25 W. The temperature is monitored by a platinum resistor in contact with the sample holder. After sample mounting, the resistor indication is compared with the temperature reading of an infrared pyrometer by a preliminary calibration in an auxiliary UHV chamber. The sample holder can also be cooled by liquid-nitrogen circulation in a thin-walled stainless-steel tube set around the molybdenum ring: We measure temperatures of about 120 K on the molybdenum block.

2. Sample preparation

The experiments reported here have been performed on two different samples.

Sample 1. Taken from a C-31034 RCA photomultiplier tube, p-doped with zinc ($\sim 10^{19}$ cm^{-3}) and oriented along the (100) face.

Sample 2. Purchased from M/A-Com Laser Diode Inc., zinc doped in the range $0.7-1.6\times 10^{19}$ cm^{-3}, oriented along the (100) face.

Before installing the sample into vacuum, we use a chemical cleaning in a 1:1:4 solution of H_2O, H_2O_2 30%, and H_2SO_4 followed by concentrated HF etching.[2,8] The sample is heat cleaned in vacuum, the temperature being limited by the maximum congruent evaporation temperature of gallium and arsenic under the Langmuir condition (~ 660 °C).[31] The activation is then performed, under He-Ne laser illumination, by cesium (generated by a commercial dispenser operating in the low 10^{-10}-Torr range) and oxygen (introduced through a microleak at a pressure in the low 10^{-9}-Torr range) coadsorption.

3. Photoemission performances

The efficiency of our photocathodes can be compared to the results quoted in the literature from the typical yield curve presented in Fig. 2. The data are obtained on sample 2 excited by the different Kr^+-laser lines in energy analysis conditions. For sample 1, the yields are ~ 2 times smaller. Our best efficiencies are about 2 times higher than those reported in Fig. 2. With no cesium excess and no permanent activation during the measurements, which are our experimental conditions, the total emitted current decreases with time at a rate of about 1%/h (see Sec. IV B 1).

III. THEORETICAL BACKGROUND

In this section we shall recall some fundamental properties of GaAs which will be useful to interpret the EDC data of Sec. IV.

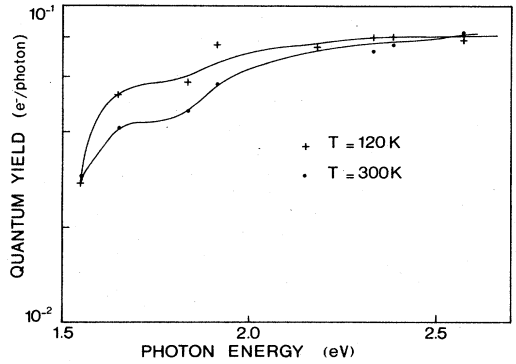

FIG. 2. Typical yield curves measured at 300 and 120 K on sample 2, using most of the Kr^+-laser lines.

A. GaAs band properties

1. Bulk properties

Gallium arsenide is a direct-band-gap semiconductor: Photoexcitation of electrons from the valence bands into the conduction band requires conservation of both wave vector $\vec{k}$ and energy; i.e., absorption of light with energy somewhat greater than the band gap E_G induces vertical transitions. The band-gap width varies with temperature: $E_G=1.42$ eV at 300 K, $E_G=1.50$ eV at 120 K (all the GaAs data we quote are taken from Blakemore's review, Ref. 32). Figure 3 shows the GaAs band structure along particular directions of the Brillouin zone, after Chelikowsky and Cohen.[33] Using Koster *et al.* notations,[34] the symmetries of the states at the zone center Γ are Γ_6 for the conduction band, Γ_8 for the degenerate valence bands split by the spin-orbit energy $\Delta=0.34$ eV (temperature independent) from the Γ_7 spin-orbit-split valence band. The conduction band presents subsidiary minima at the L points [$\vec{k}=(2\pi/a)(\frac{1}{2},\frac{1}{2},\frac{1}{2})$, where a is the cubic lattice constant] and at the X points [$\vec{k}=(2\pi/a)(1,0,0)$]. The Γ-L and Γ-X energy spacings vary slightly with temperature (less than 10 meV between 300 and 120 K) and are, respectively, 300 and 470 meV at 120 K.

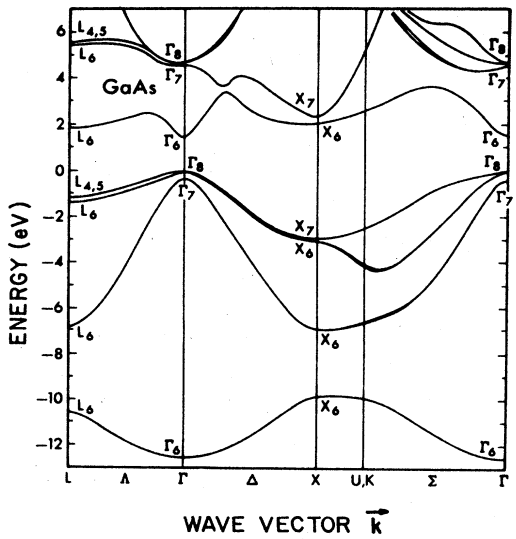

FIG. 3. GaAs band structure, after Chelikowsky and Cohen (Ref. 33). The energy origin is at the maximum of the upper valence bands (Γ_8).

2. Interface

Near the surface of heavily p-type doped GaAs, the bands are bent downwards by an amount $\delta V\simeq 0.5$ eV because of the Fermi-level pinning at approximately one-third of the band gap.[35] The band bending takes place within a distance:

$$l_D \sim \left[\frac{2\epsilon_0\epsilon_r}{(N_a-N_d)e^2}\delta V\right]^{1/2}, \tag{2}$$

where $\epsilon_0\epsilon_r$ is the dielectric permittivity of the crystal, N_a (N_d) the acceptor (donor) concentration. For a photoemitting material, p-type doped in the range 10^{19} cm^{-3}, $l_D\sim 100$ Å. The parameters of the semiconductor-vacuum interface are sketched in Fig. 4; Φ is the GaAs work function, i.e., the energy difference between the Fermi level E_F and the vacuum level, χ the electron affinity (i.e., the energy difference between the bottom of the conduction band near the *surface* and the vacuum level), and χ_A the *effective*-electron affinity (i.e., the energy difference between the bottom of the conduction band in the *bulk* crystal and the vacuum level).

B. NEA GaAs photoemission

Our photoemission experiment can be described by the well-known three-step process:[36–38] (i) photoexcitation of electrons into the conduction band; (ii) energy relaxation and transport to the surface; (iii) emission into vacuum. We briefly recall the basic features of each step.

(i) When the photon energy $h\nu$ is such that $E_G\leq h\nu<E_G+\Delta$, transitions occur between the heavy-hole band (noted Γ_{8h}) or the light-hole band (Γ_{8l}) and the conduction band (Γ_6). For $h\nu\geq E_G+\Delta$ transitions from the spin-orbit-split valence band (Γ_7) also become possible. We shall, respectively, label these transitions as $\Gamma_{8h}\rightarrow\Gamma_6$, $\Gamma_{8l}\rightarrow\Gamma_6$, and $\Gamma_7\rightarrow\Gamma_6$. Note that in our experimental conditions, where $h\nu$ varies from 1.55 to 2.60 eV, all the transitions occur in the "vicinity" of the zone

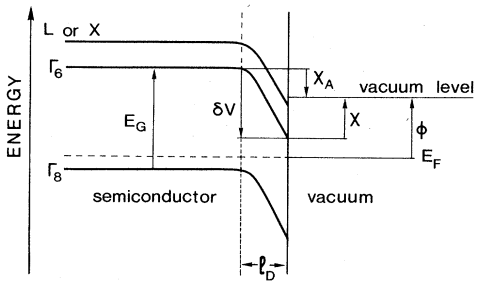

FIG. 4. Parameters of the semiconductor-vacuum interface (see Sec. III A 2). The energy levels are schematized versus the distance to the semiconductor surface.

center [$|\vec{k}| < \frac{1}{6}(2\pi/a)$]. The optical-absorption coefficient $\alpha(h\nu)$ reflects the joint density of states of the bands involved and is roughly proportional to $(h\nu - E_G)^{1/2}$: In fact, its frequency dependence is strongly affected by exciton absorption, band tailing, and nonparabolicity of the bands. For photon energies varying from 1.55 to 2.60 eV, the absorption length $\alpha^{-1}(h\nu)$ decreases from ~ 1 to ~ 0.35 μm: it remains sufficiently large compared to l_D to ensure that the optical absorption takes place in the bulk crystal.

(ii) After excitation into the conduction band the electrons suffer energy relaxation. For the kinetic energies relevant to our experimental conditions two mechanisms govern the relaxation in the Γ valley: emission or absorption of optical phonons,[2] the energy of which is close to 30 meV, with negligible dispersion; collisions with heavy holes which are transferred to the light-hole band, a mechanism proposed, and estimated in a parabolic-band model, by D'yakonov, Perel', and Yassievich (DPY).[39] The decrease of the polar optical scattering rate in Γ with increasing energy[40] is reduced by the nonparabolicity of the conduction band and by the wave-vector dependence of the cell-periodic part of the Bloch functions.[41] The calculated[2,41] and measured[42,43] collision rate for this mechanism is $\sim 10^{13}$ s^{-1}. The efficiency of the DPY mechanism increases with hole concentration and becomes significant for $N_a - N_d > 5.10^{17}$ cm^{-3};[44] nevertheless, no accurate determination of its scattering rate is available. The two mechanisms seem of comparable probability in our experimental conditions; they essentially differ by the absence of fixed-energy decrement in the DPY process in contrast with the well-defined energy transferred in a collision with an optical phonon.

When energetically allowed, the intervalley diffusion from Γ to L or X plays a dominant role in the energy-relaxation mechanisms. Indeed the diffusion rate from Γ to L or X, about 10^{13} s^{-1},[2,42] is 1 order of magnitude larger than that of the inverse process.[2] Moreover, the collision rate in L or X is $\sim 10^{14}$ s^{-1}.[2] Whenever its energy is sufficient, an electron will finally be scattered from the central valley to the side valleys where it will rapidly relax its energy prior to rediffusion towards Γ. The L or X valleys behave as intermediate electron sources which, at low temperature, may be considered as quasimonoenergetic.[44] Before escaping into vacuum the photoelectrons have then to reach the surface. This process can be described by ballistic or random-walk models for hot electrons[45–50] or by diffusion models for thermalized ones.[20,21,37] As the reflection coefficient of the surface is high,[51] the electrons undertake many attempts before emission and may relax their energy in the band-bending region.[17,52,53] A very small fraction of the electrons photoexcited into the conduction band can, however, escape without suffering any collision. As the electron mean free path in Γ, of the order of 1000 Å (see Ref. 2 and also Sec. IV A 1 of II), remains large compared to the band-bending distance l_D, these electrons have a kinetic energy corresponding to the *bulk* creation energies from the valence bands.

(iii) For a perfect surface, electron emission into vacuum requires conservation of energy and of the wave-vector component parallel to the surface (including umklapp transitions). Following the theoretical treatment given in Ref. 37, we deduce that emission is forbidden for L minima and (100) or (110) faces. In fact, these selection rules, which assume a preserved crystal periodicity near the surface and no momentum transfer at the surface, are probably far from strict.[54,55] Moreover, the L electrons can be backscattered into Γ prior to emission. As a consequence, L structures are observed for (110) (Refs. 19–21) as well as for (100) (Ref. 17) faces.

IV. HIGH-RESOLUTION ENERGY ANALYSIS

We shall now present our experimental EDC's. First, we shall discuss the spectroscopic results and identify the high-energy structures. Next we shall attempt to interpret the observed distributions from electron-energy relaxation in the bulk crystal and in the band-bending region.

A. Band-structure determination from EDC's

EDC's have been measured at different temperatures for various excitation energies. This technique allows us to distinguish between the features related to the photon energy, i.e., to final states of optical transitions, and those appearing at well-defined cathode bias voltages, due to the conduction-band minima.[25] The structures discussed here are found to be independent of the sample and of the activation process. They are thus related to GaAs intrinsic properties. Unless otherwise specified the results presented in the figures are obtained on sample 1.

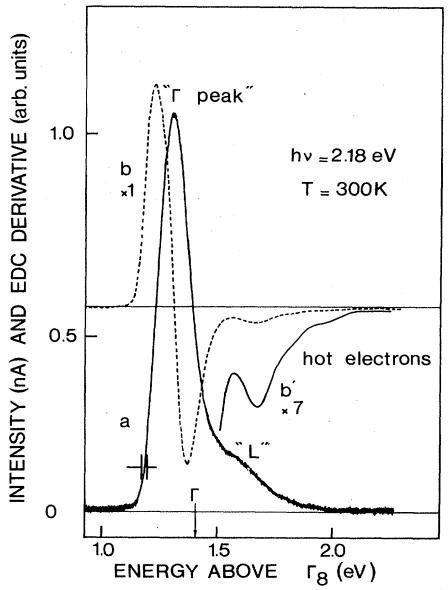

FIG. 5. EDC (curve a) and EDC derivatives (curves b and b') at 300 K of electrons emitted from NEA GaAs [(100), p-type $\sim 10^{19}$ cm^{-3}] for 2.18-eV excitation energy. The ordinate is the selector output current; electron energy is referred to the valence-band maximum Γ_8. The experimental resolution is represented by ⊣⊢ . The arrow indicates the bulk Γ position, determined by the energy calibration described in Sec. IV A 1. The notations "Γ peak," "L," and hot electrons correspond to the observed structures.

Figure 5 shows an EDC and its derivative recorded for a photon energy $h\nu=2.18$ eV at 300 K. The following typical features are observed: An intense low-energy peak (the so-called "Γ peak"), lying at an energy lower than the bulk Γ position, due to electrons which, in the *bulk* crystal, were thermalized at the bottom of the conduction band. Its exact shape depends on the position of the vacuum level which acts as a high-pass-energy filter and truncates the low-energy part of the EDC (see Sec. IV B 1); higher-energy shoulders originating either from electrons relaxed in the side valleys (L in the case of Fig. 5) or from final states of optical transitions.

1. Energy calibration

At low temperature (Fig. 6), all structures become sharper and as energy gain is much less probable than energy loss during a collision, a steep starting point is observed on the high-energy side of the EDC derivative (Γ_{8h} point in Fig. 6, curve b'). It corresponds to the initial energy of an electron promoted from the heavy-hole band into the conduction band by absorption of a photon of energy $h\nu$, i.e., to the final state of the $\Gamma_{8h}\rightarrow\Gamma_6$ transition, and provides an accurate voltage reference on the energy axis of the EDC. Its position shows up an almost linear variation as a function of $h\nu$ with the slope 0.84 over our whole energy range (compare with the Γ_{8h} data of Fig. 9). In the simple model of parabolic bands, the electron initial energy ϵ_i is given by $\epsilon_i=(h\nu-E_G)(1+m_c^*/m_{\rm hh}^*)^{-1}$, where, m_c^* ($m_{\rm hh}^*$) is the conduction (heavy-hole) mass; the predicted slope versus $h\nu$, 0.88,[32] is indeed observed for $h\nu\leq 1.9$ eV. The voltage reference is carried over to the room-temperature results taking into account the variations of the band gap, of the Fermi energy E_F, and using temperature-independent effective masses, a reasonable approximation.[56] Indeed, if we note $V_M(h\nu)$, the cathode bias potential applied to select these most energetic electrons and make use of relation (1), we obtain

$$eV_M(h\nu)\simeq h\nu(1-m_c^*/m_{\rm hh}^*)-E_F+(m_c^*/m_{\rm hh}^*)E_G-\Phi\ . \tag{3}$$

Because of conduction-band nonparabolicity this energy calibration is only correct for $h\nu$ close to E_G. The extrapolation of the Γ_{8h} point to $h\nu=E_G$ provides the position on the energy axis of the Γ minimum in the bulk. It is labeled Γ in the figures. For larger photon energies, we shall use a more appropriate description of the band structure and verify the perfect consistency of all energy determinations.

2. EDC's analysis

We now consider the EDC data as a function of exciting photon energy $h\nu$ and focus our attention on the high-energy low-temperature results. Figure 7 presents EDC derivatives at 120 K for various Kr^+-laser lines and for fairly low light power (~ 0.2 W cm^{-2}). The low-

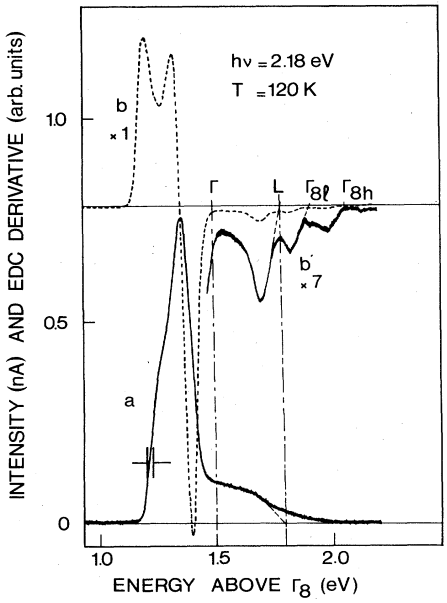

FIG. 6. EDC (curve a) and EDC derivatives (curves b and b') at 120 K, for the same excitation energy as that of Fig. 5. The bulk Γ and L locations, marked by the dot-dashed lines, are evidenced, as well as the creation energies from the light-hole (Γ_{8l}) and heavy-hole (Γ_{8h}) bands. The extrapolation procedure of Sec. IV A 2 is shown for Γ_{8h}, Γ_{8l} creation energies, and L position determinations.

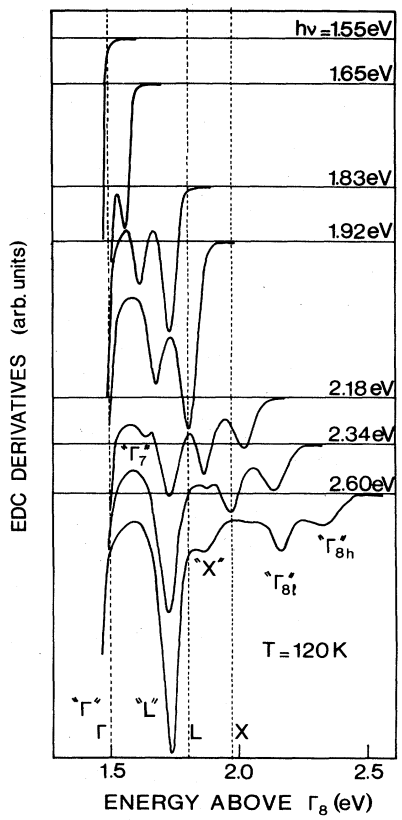

FIG. 7. EDC derivatives at 120 K for most of the Kr^+-laser lines. The bulk Γ, L, and X positions are indicated by the dotted lines. The peaks observed on the EDC derivatives are labeled "Γ," "L," "X," "Γ_7," "Γ_{8l}," and "Γ_{8h}".

energy parts of the curves have been omitted for clarity; the sharp slopes on the left-hand side correspond to the high-energy tail of the "Γ peak." This figure evidences the two types of structures already mentioned: three structures, labeled "Γ," "L," "X" do not depend on photon energy while three others ("Γ_{8h}," "Γ_{8l}", "Γ_7"), vary with $h\nu$.

Under steady-state photoexcitation, electrons accumulate at the bottom of the conduction-band minima [see (ii) of Sec. III B]. A simplifying model is to consider the quasithermalized states in these minima as quasimonoenergetic electron sources, on equal footing with the final states of the optical transitions. The electrons then relax their energy so that, at 120 K, the different features are spread towards lower energies and only their high-energy thresholds correspond to one of these electron sources. As the EDC derivatives essentially consist of discrete overlapping peaks (i.e., each source gives rise to plateaus on the EDC's), we determine these particular energies by extrapolating the high-energy slope of the structures on the EDC derivatives (Fig. 6, curve b'). Such a procedure may appear somewhat unusual: In high-energy photoemission experiments, such as those using synchrotron radiation, secondary electron excitation is the predominant energy-relaxation mechanism. The energy losses during a collision (at least the band-gap energy) are generally so important that the higher-energy structures of the EDC's are characteristic of the densities of states.[57] In contrast, in our case, where a much smaller portion of the Brillouin zone is explored, the energy relaxation of electrons, which occurs by small steps, determines the shape of the EDC structures. As a consequence only the high-energy thresholds of the experimental features are related to the energy dispersion curves.

From the positions of the high-energy edges of the $h\nu$ independent structures we deduce energy separations of 300 meV between Γ and L, and of 460 meV between Γ and X; the uncertainties are of the order of the experimental resolution (20 meV). These values are in excellent agreement with the values quoted in the literature.[32]

A parabolic-band model proved inadequate to identify the photon-energy-dependent structures. As for the heavy-hole-band warping, it leads to a maximum dispersion in the electron-promotion energy of the order of 30 meV for $h\nu=2.60$ eV,[58] our largest photon energy, and we neglect it. Therefore we use the isotropic second-order $\vec{k}\cdot\vec{p}$ Kane model[59] to analytically describe the GaAs band structure. In this model, the $\vec{k}\cdot\vec{p}$ perturbation and spin-orbit interaction are first exactly diagonalized in the quasidegenerate conduction- and valence-band subset; the remote band coupling is then added as a perturbation.[60,61] The most striking feature is a vanishing coupling between Γ_{8l} and Γ_7 bands when the light-hole kinetic energy becomes of the order of 0.5Δ. This leaves two parallel Γ_{8h} and Γ_{8l} bands separated by $\simeq 2\Delta/3$ (see Fig. 8). For our energy resolution, nonparabolicity must be considered in the conduction band at kinetic energies larger than Δ, in agreement with the conclusions drawn in Sec. IV A 1.

From the calculated valence and conduction bands, we determine the GaAs structure diagram, i.e., the electron-promotion energies from the three valence bands versus

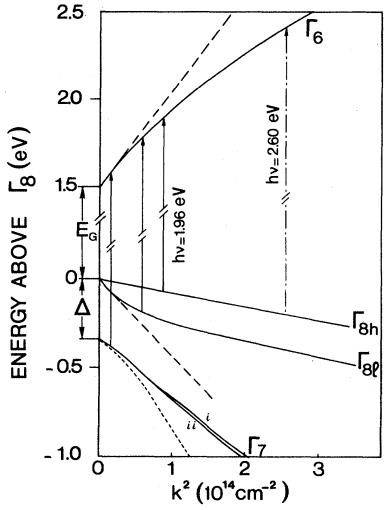

FIG. 8. GaAs band structure around the Brillouin-zone center versus squared wave vector k^2 at 120 K. The lowest conduction band Γ_6 and the three highest valence bands Γ_{8h}, Γ_{8l}, and Γ_7 are visualized. The dashed lines represent the parabolic approximation, the solid ones are calculated from the spherical nonparabolic Kane band model (Ref. 59). The only notable modification of this band set when the interband matrix element P^2 varies from 28.8 to 22 eV concerns the Γ_7 band (curve i: $P^2=28.8$ eV; curve ii: $P^2=22$ eV). The dotted Γ_7 band is the result of the D'yakonov and Perel' valence-band model (Ref. 64). The three vertical arrows schematize the optical transitions by absorption of photons of energy $h\nu=1.96$ eV. The dot-dashed arrow limits the portion of the Brillouin zone explored in our experiments ($h\nu=2.60$ eV).

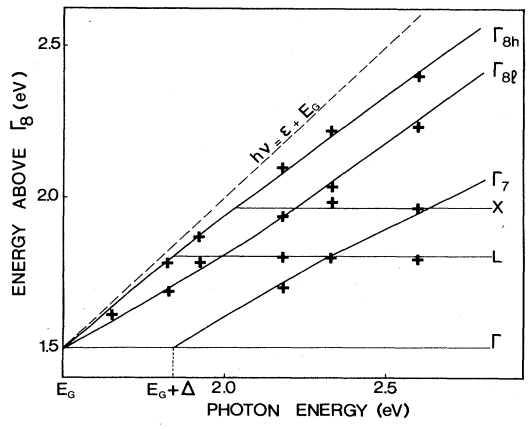

FIG. 9. GaAs structure diagram, i.e., the positions of the EDC structures as a function of the photon energy $h\nu$ at 120 K. The crosses correspond to the experimental determinations of the structure locations. The Γ_{8h}, Γ_{8l}, and Γ_7 lines are calculated in the framework of the $\vec{k}\cdot\vec{p}$ Kane model. The Γ position is deduced from an extrapolation to $h\nu=E_G$ of the position of the Γ_{8h} and Γ_{8l} promotion energies (see Secs. IV A 1 and IV A 2). The experimental X and L locations are indicated by horizontal lines. The $h\nu=\epsilon+E_G$ straight line indicates the highest possible electron kinetic energy ϵ for a given $h\nu$ (the Einstein limit; Ref. 25).

$h\nu$, at $T=120$ K (Fig. 9). The crosses refer to our experimental determinations. We unambiguously assign the three energy-dependent structures to the final states of the $\Gamma_{8h}\rightarrow\Gamma_6$ (heavy-hole structure), $\Gamma_{8l}\rightarrow\Gamma_6$ (light-hole structure) and $\Gamma_7\rightarrow\Gamma_6$ (spin-orbit structure) transitions, respectively. The agreement between the prediction and the experiment is excellent. Note that an extrapolation of the positions of the $\Gamma_{8h}\rightarrow\Gamma_6$ and $\Gamma_{8l}\rightarrow\Gamma_6$ transitions to a photon energy $h\nu=E_G$ determines the bulk Γ position very accurately.

In Fig. 7 the $\Gamma_{8l}\rightarrow\Gamma_6$ transition appears at a photon energy $h\nu\geq 1.83$ eV, when the Γ_{8l} and Γ_{8h} bands become parallel, leading to comparable densities of states in these two bands. The $\Gamma_7\rightarrow\Gamma_6$ transition is only observed for excitation at $h\nu=2.18$ eV: for a smaller $h\nu$, this structure would be weaker (due to the lower density of states in the Γ_7 band) and very close to the main "Γ peak." At $h\nu=2.34$ or 2.60 eV it is too close to L (~ 10 meV) or X (~ 40 meV) to be observable.

At room temperature, qualitatively the same results are obtained (Fig. 10) but the structures are not so sharp and, as energy gain or loss during collision become equally probable, their energy positions cannot be accurately measured. Some features even disappear, such as the heavy-hole structure at $h\nu=1.65$ eV, the spin-orbit structure at $h\nu=2.18$ eV, or the X structure. However, identifications can be carried out in good agreement with the above band-structure calculation provided that the variation of E_G with temperature is taken into account.

High-energy photoemission currently probes band structures throughout the Brillouin zone. But for near-band-gap energies, this work presents the first direct and accurate experimental determination of the GaAs band structure in the vicinity of the Γ point. This has been possible by using both a high-resolution electron-energy analyzer and a well-focused laser as a light source. This technique yields more straightforward information than magneto-optical experiments for which excitonic effects make the interpretation intricate[62,63] and is a test for band-structure models. For example, an alternative to Kane's $\vec{k}\cdot\vec{p}$ calculation was proposed by D'yakonov and Perel' (DP):[64] they determine the three valence bands from symmetry arguments and do not favor the coupling to the Γ_6 conduction band; the parameters of their model are deduced from the experimental heavy- and light-hole masses at the Brillouin-zone center. The predicted Γ_7 bands are quite different in DP and Kane models (see Fig. 8) and photoemission experiments in which the "Γ_7" structure would be resolved from the "X" one ($h\nu>2.7$ eV) should discriminate between these two descriptions.

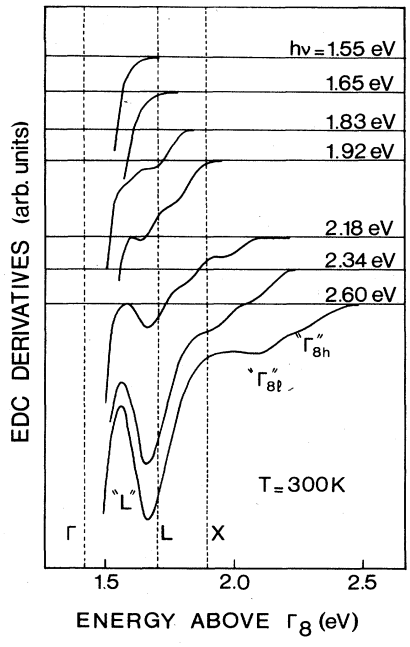

FIG. 10. EDC derivatives at 300 K for most of the Kr^+-laser lines. The bulk Γ position is deduced from the 120-K calibration (see Sec. IV A 1). The bulk L and X locations, calculated from our 120-K determinations and the temperature variation of Ref. 32, are indicated by dotted lines. The peaks observed on the EDC derivatives are labeled "L," "Γ_{8l}," and "Γ_{8h}."

B. Energy relaxation and surface effects

After identification of all the bulk structures occurring in the EDC's, we now study the photoemitted distribution and the band-bending effects.

1. Low-energy part of the EDC's

We first consider the low-energy part of the EDC's originating from electrons which were thermalized at the bottom of the conduction band in the bulk crystal before being emitted. As the low-energy slope of the EDC's corresponds to an affinity cutoff, we must be cautious in re-

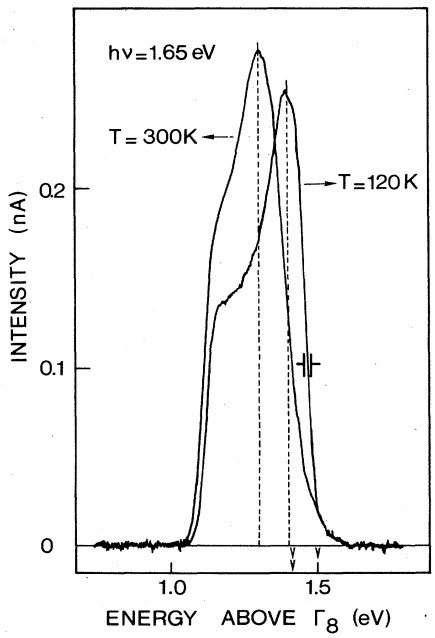

FIG. 11. EDC's at 300 and 120 K for $h\nu=1.65$ eV. The temperature variation of the "Γ peak" (dashed lines) is evidenced. The symbol V ($\overset{V}{V}$) on the energy axis shows the bulk Γ location at 120 K (300 K). Note the low-energy shoulders due to the very low, almost temperature-independent, vacuum level.

lating the position of the "Γ peak" to the bulk band structure. Fortunately, for very low affinity photocathodes, we observe an additional lower-energy shoulder (at 300 K as well as at 120 K, see Fig. 11) or even a lower-energy peak (see Fig. 8 of II). Such a shoulder, already mentioned in Refs. 20 and 21, was attributed to surface reflections of electrons from the main peak. This extra structure ensures that the "Γ peak" is not upshifted by affinity cutoff. Thus, we measure its location, at $\simeq$130 meV below the energy of the bulk Γ minimum, almost independently of temperature and of sample. A shift was also reported for GaP,[65] GaAs,[17,52] $Ga_{1-x}In_xAs$,[52] and $GaAs_{1-x}P_x$.[53] Its origin is not clearly established. It could originate from (i) scattering of Γ electrons into the bottom of the L valley in the band-bending region, a mechanism suggested by James and collaborators[20,21] to explain the FWHM of the "Γ peak"; (ii) accumulation in quantized levels in the band-bending well,[52] which seems unplausible because of the broadening due to disorder effects;[66] (iii) energy loss when crossing the Cs layer,[21] a hardly conceivable hypothesis since we are able to produce very narrow EDC's (see Fig. 12); (iv) energy losses in the space-charge region as calculated in Ref. 67, a mechanism compatible with all present measurements.

The analysis of the low-energy end of the EDC's remains intricate and needs further investigations.

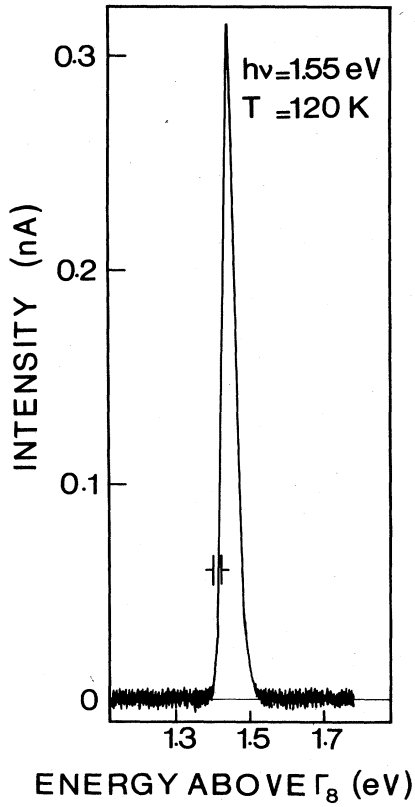

FIG. 12. Very narrow EDC ($\simeq$30-meV FWHM) recorded under near-band-gap excitation at 120 K. The sharp low-energy edge corresponds to the cutoff by the only slightly negative affinity (see Sec. V B of II). The high-energy decrease is slower and nearly Maxwellian.

Nevertheless, the sharp low-energy edges of our EDC's determine the vacuum level positions and also give a lower limit for the band-bending value: We measure effective-electron affinities as low as −0.50 eV at 120 K and −0.43 eV at room temperature. Spicer *et al.*[35] report a band bending $\delta V \simeq 0.5$ eV for the (110) face; in contrast James and collaborators[68] find $\delta V \simeq 0.23$ eV for the (110) face and 0.28 eV for the (100) face. The latter values are too small and we conclude that $\delta V \geq 0.5$ eV. Moreover, from Fig. 11 we deduce that the work function is nearly temperature independent[69,70] as can also be observed in Refs. 20 and 21. Consequently, when a GaAs photocathode is cooled, the effective-electron affinity decreases as the band gap increases. This leads to an increase in quantum efficiency (see Fig. 2). We, however, note that it usually reaches a maximum value at an intermediate temperature.[20,21,71]

The low-energy part of the EDC is directly affected by photocathode aging and surface preparation: Figure 13 shows EDC's obtained under the same experimental conditions as a function of time. We observe that the main effect is a low-energy cutoff due to the rise of the vacuum level, thus leading to a decrease of the total emitted current. This aging process can be attributed either to cesium desorption (mainly at room temperature where the initial yield is almost restored by adding cesium) or to surface pollution (mainly at lower temperature, due to cryopumping of residual gases, where warming up the cathode again restores most of the initial efficiency). The exact rate of decrease of the photocurrent depends on the shape of the distribution: The affinity rises almost linearly, by about 10^{-1} eV per day in our experiments. We also verified that a nonoptimum surface preparation (insufficient

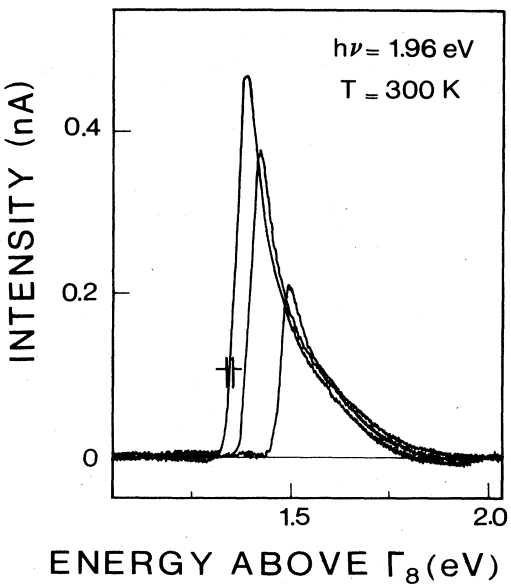

FIG. 13. EDC time evolution under given temperature and light excitation conditions. The time elapsed between the extreme recordings is of the order of 1 d with a pressure in the low 10^{-10}-Torr range. The rise of the electron affinity, evident on the figure, decreases the total emitted current (proportional to the area under each curve).

heat cleaning, Cs or O_2 excess) only leads to a vacuum level cutoff at higher energy.

It was pointed out[20,21] that the photoemission peak positions could be upshifted because of the electron-energy dependence of the semiconductor-vacuum interface transmission coefficient. This effect can be neglected when the energy dependence is sufficiently weak, which is generally the case. However, it should be observable for electrons of energy close to that of the vacuum level as the transmission coefficient shows a rapid variation with energy. We indeed observe an additional shift towards higher energies of the low-energy peak in Fig. 13 as the work function increases.

2. *High-energy tail of the "Γ peak"*

At energies larger than the Γ minimum in the bulk crystal, the high-energy tail of the "Γ peak" is Maxwellian, with an effective temperature T_e larger than the lattice temperature T. At a given lattice temperature, T_e increases with the photon energy $h\nu$, in agreement with the results of James and collaborators[20,21] and is not very much sample dependent. For $h\nu=1.55$ eV, $k_B T_e$ is of the order of 20 meV at 120 K and $\simeq$40 meV at 300 K, where k_B is the Boltzmann constant; the effective temperatures are doubled for $h\nu \geq 1.92$ eV. These results are to be compared with the luminescence line shapes that we obtain on the same samples under the same light excitation power: At liquid-nitrogen temperature and for $h\nu=1.92$ eV, we find $k_B T_e \sim 10$ meV. Broadened luminescence lines were already reported,[72,73] but for higher excitation powers. The increase with $h\nu$ of the width of the photoemitted electron distribution can be qualitatively understood: On the one hand, the electrons have more energy to lose, so that their complete thermalization would require a longer time. On the other hand, because of the increased absorption coefficient, they are excited closer to the crystal surface, i.e., on the average they spend less time in the crystal before emission. An additional broadening may result from heating in the band-bending region.[67]

3. *Side valleys*

In our conditions, the side valleys give rise to plateaus rather than to peaks. At low temperature, a broad L peak seldom occurred at an energy $\simeq$220 meV under the location of the bottom of the bulk L minimum.[52] Spin-polarization measurements (see Sec. IV B 3 of II) show that the L and X plateaus are due to electrons having undergone energy relaxation in the L or X band bending rather than backscattered in the Γ valley of the bulk crystal.

4. *Influence of doping level*

No optical-phonon oscillation is observed on the high-energy part of the EDC's. This can be expected because at our doping levels the DPY mechanism, in which the energy-loss value is not defined, is probably more efficient than optical-phonon emission to relax the electron energy.[39] The situation is the same for hot photoluminescence where such oscillations are seen only for p-type doped samples with $N_a - N_d < 5.10^{17}$ cm^{-3}.[44] Systematic investigations of photoemission as a function of doping should clarify the influence of the band-bending region and of the different energy-relaxation mechanisms.

C. Comparison with the results of James and collaborators

High-resolution energy analysis of electrons photoemitted from a (110) cleaved GaAs face activated to negative electron affinity was thoroughly studied in the pioneer papers of James and collaborators.[19–21] This work was a breakthrough in the experimental as well as theoretical understanding of NEA GaAs photoemission and has remained unquestioned for 15 years. It was all the more remarkable as their experiments were performed using a retarding field electron analyzer and a filtered lamp for light excitation. Moreover, the GaAs band structure was not so accurately established: Before Aspnes *et al.* reordering,[74,75] the bottom of the X valleys was thought to lie lower in energy than that of the L valleys. It is presently established that the reverse situation occurs. In particular, James and collaborators results must be reinterpreted in this way: In the following, we call L (respectively, X) the valleys noted X (respectively, L) in their work. In this section we compare our results to those of James and collaborators, as well as comment and discuss their interpretations.

1. *Quantum yield*

The first expected information on a photocathode is its quantum yield $Y(h\nu)$. James and collaborators[20,21] have shown that a diffusion model allows the determination of the diffusion length and the electron escape probability in Γ (and in a similar manner in L or X) using a plot of $1/Y(h\nu)$ as a function of $1/\alpha(h\nu)$. This method requires an accurate determination of the quantum yield and a very precise knowledge of the absorption coefficient of GaAs for near-band-gap excitation, where band tailing effects are important. Moreover, some additional hypotheses have to be done in order to separate the respective contributions from the Γ, L, and X minima to the total quantum yield. This diffusion model takes into account the influence of the band-bending region as a whole through the escape probability: information is not provided for either the transport process in the band-bending region or for the position of the vacuum level. Carefully using this model, James and collaborators deduce Γ escape probabilities of the order of 20% and Γ diffusion lengths $\simeq 1.6\ \mu$m. We only qualitatively use this method and roughly estimate Γ escape probabilities up to 10% and diffusion lengths smaller than, or of the order of 1 μm in fair agreement with their results.

2. *Energy resolution and calibration*

The major experimental improvements between James and collaborators experiments and ours are the much better energy resolution and reliability of our spectrometer and the use of laser excitation. A well-focused light spot prevents averaging over regions with different work func-

tions; it leads to a more accurate description of the lower-energy part of the EDC's. James and collaborators do not specify the energy resolution of their analyzer but, from their results, we evaluate it to ~ 100 meV. They do not detail their energy calibration and position the Γ bulk minimum very close to the low-energy peak ("Γ peak"). Their procedure leads to finding a sizable contribution of electrons at energies exceeding $h\nu$, which casts some doubts on their energy scale; Fig. 4 of Ref. 19 at $h\nu=2.2$ eV has to be compared to Fig. 5 of this paper, for which $h\nu=2.18$ eV. On the contrary, we prove that the "Γ peak" is down shifted by 130 meV with respect to the Γ minimum in the bulk. James and collaborators,[20,21] however, determine the correct temperature variation of the band gap since the "Γ peak" shift is almost temperature independent.

3. *Conduction-band structures*

In papers by James and collaborators, an important L peak is reported; generally we only obtain a plateau. It is not clear whether this discrepancy is due to the emitting face orientation, to quality differences between our heat-cleaned faces and their UHV cleaved faces, or to differences in the energy analysis techniques. At 80 K, they measure a Γ-L energy spacing of about 350 meV, which agrees with our determination within 50 meV. This is fortuitous since the "Γ peak" is shifted into the band-bending region by $\simeq 130$ meV. A similar low-energy shift, but of a somewhat different quantity (220 meV), was also observed for the L peak[52] in agreement with our experiments. James[21] obtains an L-X spacing of 80 meV at room temperature, in contradiction with the value calculated from Ref. 32 (190 meV). In fact, in the experiments of Refs. 19 and 21, the location of the very weak X structure cannot be accurately determined.

4. *Final states: hot-electron structures*

Because of our improved resolution we obtain a much more detailed picture of the band structure of GaAs, separating the final states of optical transitions over our whole photon energy range. A confusing point in the work of James and collaborators is that, at $h\nu=2.2$ eV for $T=300$ K, two structures labeled "final states" (that we assign to $\Gamma_{8h}\rightarrow\Gamma_6$ and $\Gamma_{8l}\rightarrow\Gamma_6$ transitions) are observed in Ref. 19 whereas only a single broad structure ("hot-electron structure") is reported in Refs. 20 and 21 for $h\nu\geq 2.3$ eV and attributed to hot-electron relaxation. For $h\nu>2.60$ eV, the situation becomes still more intricate, as the subsidiary minimum X_{7c} of the second conduction band, which lies at 870 meV above Γ (Refs. 32 and 33) can also be populated.[75] Indeed, James and collaborators observe a $h\nu$ independent peak located 810 meV above Γ in Fig. 1 of Ref. 20, which is assigned to the X_{7c} valleys in Ref. 21. Yet it is in this very energy region that they deduce the hot-electron mean free path from a fit of the hot-electron structure in a random-walk model (see Fig. 9 of Ref. 20 and Fig. 21 of Ref. 21). From our analysis, we conclude that, if such a structure exists, it should be masked by the X_{7c} one at $h\nu>2.6$ eV. For $1.83\text{ eV}\leq h\nu\leq 2.6$ eV we always separate the $\Gamma_{8h}\rightarrow\Gamma_6$ and $\Gamma_{8l}\rightarrow\Gamma_6$ transitions. We think that the hot-electron structure observed in Refs. 20 and 21 originates from the two unresolved $\Gamma_{8h}\rightarrow\Gamma_6$ and $\Gamma_{8l}\rightarrow\Gamma_6$ transitions when $h\nu\leq 2.6$ eV and also from the contribution of the X_{7c} minimum when $h\nu>2.6$ eV. As a consequence it seems impossible to calculate transport parameters for hot electrons in the way given in these papers. Yet, all the experimental data of James and collaborators can be consistently reinterpreted within our analysis.

V. CONCLUSION

EDC'S of NEA GaAs photocathodes are measured with an energy resolution of 20 meV under focused laser excitation. For the first time, the GaAs conduction- and valence-band structure in the "vicinity" of the Γ point $[|\vec{k}|<\frac{1}{6}(2\pi/a)]$ is *directly* investigated; a $\vec{k}\cdot\vec{p}$ perturbation model including nonparabolicity perfectly fits the experimental data. The energy positions of the conduction-band extrema are determined and found in excellent agreement with band-structure calculations.[33] This study confirms the previous experimental results of James and collaborators,[19–21] yet our analysis leads to a reexamination of their conclusions. In particular, we demonstrate that a determination of the hot-electron mean free path from photoemission measurements as proposed in Refs. 20 and 21 is not possible. We verify that, in NEA photocathode, the major part of the emitted current originates from electrons thermalized at the Γ minimum of the conduction band in the bulk solid and having suffered additional energy relaxation in the band-bending region.[17,52,53,65] We show that the loss of efficiency occurring with aging of the photocathode is mainly due to a cutoff of the low-energy part of the main peak, indicating a rise of the electron affinity.

The exact shape of the EDC's at energies lower than the Γ minimum in the bulk crystal must still be studied in more detail, especially for very negative electron affinities, but the main features of the EDC's are now well understood. This work clearly demonstrates that high-resolution energy analysis on activated semiconductors is a powerful tool to investigate bulk and surface properties.

ACKNOWLEDGMENTS

We gratefully acknowledge the participation of M. Eminyan at the initiation and during the early stages of this experiment. We are indebted to D. M. Campbell for useful advice and to D. Paget for pertinent remarks on the manuscript. We have benefited from helpful discussions with J.-N. Chazalviel, G. Fishman, J. F. Gouyet, J.-P. Hermann, R. Houdré, P. Jarry, D. Paget, C. Piaget, and A. Tardella. We thank C. Vasseur for technical help. One of us (H.-J.D.) wishes to express his thanks to the Mission Recherche de la Delégation Générale pour l'Armement and to the Direction des Recherches, Etudes et Techniques which made it possible for him to accomplish this work. We thank Professor M. L. Cohen for permitting us to reproduce the figure on GaAs band structure (Fig. 3 of this paper). Laboratoire de Physique de la Matière Condensée is Groupe de Recherche 050038 du Centre National de la Recherche Scientifique.

[1]J. J. Scheer and J. Van Laar, Solid State Commun. **3**, 189 (1965).
[2]C. Piaget, thèse de Doctorat d'Etat, Université de Paris—Sud, Centre d'Orsay, 1977, and references therein.
[3]E. L. Garwin, D. T. Pierce, and H. C. Siegmann, Swiss Physical Society Meeting, Bern [Helv. Phys. Acta **47**, 393 (1974)].
[4]G. Lampel and C. Weisbuch, Solid State Commun. **16**, 877 (1975).
[5]D. T. Pierce, F. Meier, and P. Zürcher, Appl. Phys. Lett. **26**, 670 (1975).
[6]D. T. Pierce and F. Meier, Phys. Rev. B **13**, 5484 (1976).
[7]B. Reihl, M. Erbudak, and D. M. Campbell, Phys. Rev. B **19**, 6358 (1979).
[8]D. T. Pierce, R. J. Celotta, G.-C. Wang, W. N. Unertl, A. Galejs, C. E. Kuyatt, and S. R. Mielczarek, Rev. Sci. Instrum. **51**, 478 (1980).
[9]C. Y. Prescott *et al.*, Phys. Lett. B **77**, 347 (1978).
[10]C. Y. Prescott *et al.*, Phys. Lett. B **84**, 524 (1979).
[11]P. Souder *et al.*, in *High Energy Spin Physics—1982* (Brookhaven National Labs), edited by G. M. Bunce (AIP, New York, 1982), p. 574.
[12]E. Reichert, in Ref. 11, p. 580.
[13]A. B. McDonald, E. D. Earle, and E. T. H. Clifford, in Ref. 11, p. 586.
[14]M. Eminyan and G. Lampel, Phys. Rev. Lett. **45**, 1171 (1980).
[15]K. Bartschat, G. F. Hanne, and A. Wolcke, Z. Phys. A **304**, 89 (1982).
[16]For a review, see D. T. Pierce and R. J. Celotta, J. Vac. Sci. Technol. A **1**, 1119 (1983).
[17]H.-J. Drouhin, C. Hermann, M. Eminyan, and G. Lampel, J. Phys. (Paris) Lett. **44**, L1027 (1983).
[18]R. Azria, P. Girard, and J. P. Ziesel (private communication).
[19]L. W. James, R. C. Eden, J. L. Moll, and W. E. Spicer, Phys. Rev. **174**, 909 (1968).
[20]L. W. James and J. L. Moll, Phys. Rev. **183**, 740 (1969).
[21]L. W. James, Solid State Electronics Laboratory (Stanford University) Technical Report No. 5221-2, 1969 (unpublished).
[22]V. I. Zemskii, B. P. Zakharchenya, and D. M. Mirlin, Pis'ma Zh. Eksp. Teor. Fiz. **24**, 96 (1976) [JETP Lett. **24**, 83 (1976)].
[23]H.-J. Drouhin, thèse de Docteur-Ingénieur, Université de Paris—Sud, Centre d'Orsay, 1982.
[24]H.-J. Drouhin, C. Hermann, M. Eminyan, and G. Lampel, in *Proceedings of the 17th International Conference on the Physics of Semiconductors, San Francisco, 1984,* edited by D. J. Chadi (Springer, New York, in press).
[25]W. E. Spicer and R. C. Eden, in *Proceedings of the 9th International Conference on the Physics of Semiconductors, Moscow, 1968,* edited by S. M. Ryvkin (Nauka, Leningrad, 1968), p. 65.
[26]H.-J. Drouhin, C. Hermann, and G. Lampel, following paper Phys. Rev. B **31**, 3872 (1985).
[27]R. Herzog, Z. Phys. **89**, 447 (1934).
[28]Y. Bally, in *Applied Charged Particle Optics,* Suppl. 13B of *Advances in Electronics and Electron Physics,* edited by A. Septier (Academic, New York, 1980), p. 257, and references therein.
[29]P. Marmet and L. Kerwin, Can. J. Phys. **38**, 787 (1960).
[30]H.-J. Drouhin, M. Eminyan, C. Hermann, and G. Lampel (unpublished).
[31]B. Goldstein, D. J. Szostak, and V. S. Ban, Surf. Sci. **57**, 733 (1976).
[32]J. S. Blakemore, J. Appl. Phys. **53**, R123 (1982).
[33]J. R. Chelikowsky and M. L. Cohen, Phys. Rev. B **14**, 556 (1976).
[34]G. F. Koster, J. O. Dimmock, R. G. Wheeler, and H. Statz, *Properties of the Thirty-Two Point Groups* (MIT, Cambridge, Mass., 1963).
[35]W. E. Spicer, P. W. Chye, P. R. Skeath, C. Y. Su, and I. Lindau, J. Vac. Sci. Technol. **16**, 1422 (1979).
[36]W. E. Spicer, Phys. Rev. **112**, 114 (1958).
[37]R. L. Bell, *Negative Electron Affinity Devices* (Clarendon, Oxford, 1973).
[38]W. E. Spicer, Appl. Phys. **12**, 115 (1977).
[39]M. I. D'yakonov, V. I. Perel', and I. N. Yassievich, Fiz. Tekh. Poluprovodn. **11**, 1364 (1977) [Sov. Phys.—Semicond. **11**, 801 (1977)].
[40]E. M. Conwell, in *High Field Transport in Semiconductors,* Suppl. 9 of *Solid State Physics,* edited by F. Seitz, D. Turnbull, and H. Ehrenreich (Academic, New York, 1967).
[41]W. Fawcett, A. D. Boardman, and S. Swain, J. Phys. Chem. Solids **31**, 1963 (1970).
[42]B. P. Zakharchenya, V. D. Dymnikov, I. Ya. Karlik, D. N. Mirlin, L. P. Nikitin, V. I. Perel', I. I. Reshina, and V. F. Sapega, in Proceedings of the 15th International Conference on the Physics of Semiconductors, Kyoto, 1980 [J. Phys. Soc. Jpn. **49**, Suppl. A, 573 (1980)].
[43]C. L. Tang and D. J. Erskine, Phys. Rev. Lett. **51**, 840 (1983).
[44]B. P. Zakharchenya, D. N. Mirlin, V. I. Perel', and I. I. Reshina, Usp. Fiz. Nauk. **136**, 459 (1982) [Sov. Phys. Usp. **25**, 143 (1982)], and references therein.
[45]D. J. Bartelink, J. L. Moll, and N. I. Meyer, Phys. Rev. **130**, 972 (1963).
[46]G. A. Baraff, Phys. Rev. **135**, A528 (1964).
[47]E. O. Kane, Phys. Rev. **147**, 335 (1966).
[48]R. N. Stuart and F. Wooten, Phys. Rev. **156**, 364 (1967).
[49]S. W. Duckett, Phys. Rev. **166**, 302 (1968).
[50]D. C. Langreth, Phys. Rev. B **3**, 3120 (1971).
[51]M. G. Burt and J. C. Inkson, J. Phys. D **10**, 721 (1977).
[52]A. L. Musatov, V. L. Korotkikh, and V. D. Shadrin, Fiz. Tverd. Tela (Leningrad) **23**, 929 (1981) [Sov. Phys.—Solid State **23**, 540 (1981)].
[53]J. Kirschner, H. P. Oepen, and H. Ibach, Appl. Phys. A **30**, 177 (1983).
[54]G. W. Gobeli, F. G. Allen, and E. O. Kane, Phys. Rev. Lett. **12**, 94 (1964).
[55]N. J. Schevchik, Phys. Rev. B **16**, 3428 (1977).
[56]A. C. Sharma, N. M. Ravindra, S. Auluck, and V. K. Srivastatva, Phys. Status Solidi B **120**, 715 (1983).
[57]F. Wooten, *Optical Properties of Solids* (Academic, New York, 1972).
[58]M. S. Skolnick, A. K. Jain, R. A. Stradling, J. Leotin, J. C. Ousset, and S. Askenazy, J. Phys. C **9**, 2809 (1976).
[59]E. O. Kane, J. Phys. Chem. Solids **1**, 249 (1957).
[60]The squared momentum matrix element P^2 between the conduction and valence wave functions in the single-group representation has been chosen as $P^2=28.8$ eV (Ref. 61). To determine the coupling with remote bands we fit, at the zone center, the experimental effective masses $m_c^*=0.067m_0$, $m_{\rm hh}^*=0.51m_0$, and the light-hole mass $m_{lh}^*=0.082m_0$, where m_0 is the free-electron mass. We derive a band structure almost insensitive to the value of P^2, for P^2 ranging between 22 eV (value obtained if m_c^* is determined by the only Γ_8 and Γ_7 valence bands) and 28.8 eV (experimental determination, Ref. 61), and a Γ_7 effective mass $m_{\rm so}^*\simeq 0.16m_0$, in good agreement with the experimental value $m_{\rm so}^*=0.154m_0$ deduced from stress-modulated magnetoreflectivity (Refs. 62 and 63).
[61]C. Hermann and C. Weisbuch, Phys. Rev. B **15**, 823 (1977).
[62]M. Reine, R. L. Aggarwal, B. Lax, and C. M. Wolfe, Phys.

Rev. B **2**, 458 (1970).
[63]M. Reine, R. L. Aggarwal, and B. Lax, Phys. Rev. B **5**, 3033 (1972).
[64]M. I. D'yakonov and V. I. Perel', Zh. Eksp. Teor. Fiz. **60**, 1954 (1971) [Sov. Phys.—JETP **33**, 1053 (1971)].
[65]B. F. Williams and R. E. Simon, Phys. Rev. Lett. **18**, 485 (1967).
[66]A. Tardella (private communication).
[67]J. S. Escher and H. Schade, J. Appl. Phys. **44**, 5309 (1973).
[68]L. W. James, G. A. Antypas, J. Edgecumbe, R. L. Moon, and R. L. Bell, J. Appl. Phys. **42**, 4976 (1971).
[69]W. Mönch, R. Enninghorst, and H. J. Clemens, Surf. Sci. **102**, L54 (1981).
[70]L. Sooncknidt, J. Bonnet, P. Masri, and L. Lassabatère, Surf. Sci. **130**, L337 (1983).
[71]B. Goldstein, Surf. Sci. **47**, 143 (1975).
[72]J. Shah and R. C. C. Leite, Phys. Rev. Lett. **22**, 1304 (1969).
[73]E. A. Meneses, N. Jannuzzi, and R. C. C. Leite, Solid State Commun. **13**, 245 (1973).
[74]D. E. Aspnes, C. G. Olson, and D. W. Lynch, Phys. Rev. Lett. **37**, 766 (1976).
[75]D. E. Aspnes, Phys. Rev. B **14**, 5331 (1976).